A Transverse Oscillation Approach for Estimation of Three-Dimensional Velocity Vectors, Part I: Concept and Simulation Study

Pihl, Michael Johannes; Jensen, Jørgen Arendt

Published in:
IEEE Transactions on Ultrasonics, Ferroelectrics and Frequency Control

Link to article, DOI:
10.1109/TUFF c .2013.006237

Publication date:
2014

A Transverse Oscillation Approach for Estimation of Three-Dimensional Velocity Vectors, Part I: Concept and Simulation Study

Michael Johannes Pihl, *Member, IEEE*, and Jørgen Arendt Jensen, *Fellow, IEEE*

***Abstract*—A method for 3-D velocity vector estimation using transverse oscillations is presented. The method employs a 2-D transducer and decouples the velocity estimation into three orthogonal components, which are estimated simultaneously and from the same data. The validity of the method is investigated by conducting simulations emulating a 32 × 32 matrix transducer. The results are evaluated using two performance metrics related to precision and accuracy. The study includes several parameters including 49 flow directions, the SNR, steering angle, and apodization types. The 49 flow directions cover the positive octant of the unit sphere. In terms of accuracy, the median bias is −2%. The precision of v_x and v_y depends on the flow angle β and ranges from 5% to 31% relative to the peak velocity magnitude of 1 m/s. For comparison, the range is 0.4 to 2% for v_z. The parameter study also reveals, that the velocity estimation breaks down with an SNR between −6 and −3 dB. In terms of computational load, the estimation of the three velocity components requires 0.75 billion floating point operations per second (0.75 Gflops) for a realistic setup. This is well within the capability of modern scanners.**

I. Introduction

Estimation of blood velocity is an important diagnostic tool in the clinic [1]. For instance, velocity magnitude in the carotid artery is a main diagnostic criterion in assessing the degree of stenosis [2], [3]. Several methods have been suggested to overcome the angle-dependency problem [4]–[6]; however, current clinical practice still relies on axial (one-dimensional) velocity estimates only [3].

Recent progress in clinical application of velocity estimation stems from commercial scanners capable of estimating 2-D velocity vectors in the scan plane. One of the implemented methods is the transverse oscillation (TO) approach [7], and the commercial implementation of this approach has been FDA approved for clinical use [8].

However, even 2-D approaches do not capture the full hemodynamics, because the blood flow exhibits complex flow patterns with velocity components in all three spatial dimensions, as studies using ultrasound [9]–[11] as well as MRI [12], [13] and computational fluid dynamics modeling [14], [15] have shown. This underlines the need for 3-D methods that can be implemented for real-time imaging, which is the scope of this paper.

Combining the need for a real-time 3-D velocity estimation method with the proven feasibility of a commercial implementation of the TO method, this paper proposes a transverse oscillation approach for the estimation of 3-D velocity vectors. The method estimates the transverse and elevation velocity components based on two pairs of double-oscillating fields and spatial quadrature sampling. With the 3-D TO method, the velocity estimation is decoupled into the three velocity components, which are obtained simultaneously and from the same data.

Various other methods have been suggested that provide the full 3-D velocity vector information. Of these, the cross-beam vector Doppler methods employing single-element transducers [4], [16], [17] are not suited for obtaining 3-D velocity vector estimates over an entire volume. The elements in the esophageal probe by Daigle *et al.* [16] had one point of beam convergence and had to be operated sequentially over several cardiac cycles. The system developed by Fox [17] for obtaining calibrated 3-D Doppler velocimetry information employed continuous-wave transmit/receivers sacrificing depth information, and the system had to be manually adjusted for a specific area of interest. The five-transducer system proposed by Dunmire *et al.* had similar challenges [4]. Newhouse *et al.* [18] suggested a two-transducer system that estimated the 3-D velocity based on a combination of the two Doppler mean frequencies and the Doppler spectral bandwidth. The main disadvantages of that system are the assumption of only one velocity in the region of interest and the dependence on the spectral broadening effect.

Several authors have suggested methods employing beamforming several lines and using cross-correlation to track the motion. The method by Bonnefous [19] requires a 2-D array transducer and five beamformers in parallel to obtain the velocity vector by means of five 1-D cross-correlations. The method works for transverse motions, but breaks down if axial motion is present because it will dominate the signal change. The approach by Hein [20] employing a triple-beam lens transducer requires detailed consideration of beamwidth and beam separation, and suffers from low SNR. The directional beamforming approach by Jensen [21] estimates the velocity by beamforming lines in the direction of the flow. The flow direction and the

Manuscript received December 17, 2013; accepted May 12, 2014. This work was supported by grant 024-2008-3 from the Danish Advanced Technology Foundation and BK Medical ApS, Denmark.

The authors are with the Center for Fast Ultrasound Imaging, Department of Electrical Engineering, Technical University of Denmark, Kgs. Lyngby, Denmark (e-mail: jaj@elektro.dtu.dk).

DOI http://dx.doi.org/10.1109/TUFFC.2013.006237

velocity are found by using cross-correlation estimators. The drawback of this approach is the larger number of calculations required for 3-D velocity estimation.

The speckle tracking approach is a widely used technique for motion estimation [22]. Speckle tracking in 2-D has been expanded to 3-D tissue motion tracking [23]. However, results from noninvasive speckle tracking for 3-D flow estimation have yet to be presented. Speckle or particle tracking is also used in the more recent ultrasonic particle image velocimetry (PIV) approach [24]–[26], but this approach requires that a contrast agent is injected into the blood stream. Reconstructed 3-D flow using ultrasound PIV has been reported [27], but results from estimating the full 3-D velocity vectors have yet to be reported. In general, the challenge with speckle tracking techniques, especially in 3-D, is the fairly high number of calculations needed. Another approach is to apply feature tracking in 3-D [28]; however, the approaches are limited by uncertainty, especially in the transverse localization of the peak, false peak detection, and the duration of the tracked feature.

The feasibility of the proposed 3-D transverse oscillation method is demonstrated in a simulation study. The method is presented in Section II, along with the performance metrics employed. Section III explains the simulation environment. The resulting estimates of 3-D velocities for various flow directions are presented in Section IV, and the results and discussion of the parameter study can be found in Section V. The conclusions are stated in Section VI. Measured results obtained in an experimental setup are presented in the companion paper [29].

II. The 3-D Transverse Oscillation Method

The idea of the 3-D transverse oscillation method is to introduce two decoupled pairs of double-oscillating fields which generate received signals affected by either the axial and transverse oscillations or by the axial and elevation oscillations. It is hypothesized that the velocity estimation can be decoupled for all three spatial dimensions. The following briefly describes the basic concept, the beamforming, the velocity estimation, the optimization of the method, the number of operations required in the velocity estimation, and the performance metrics employed to evaluate the method.

A. The Concept

The proposed method is based on the transverse oscillation approach suggested by Jensen and Munk [7] for 2-D velocity estimation; Anderson [30] suggested a similar approach.

In the 3-D case, the concept is to create double oscillating fields perpendicular to each other by employing a 2-D transducer as illustrated in Fig. 1. For the transverse and elevation directions, pairs of double-oscillating fields are generated. Each pair should ideally consist of two fields,

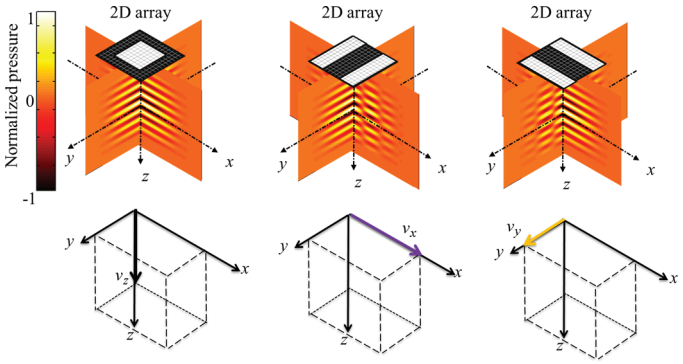

Fig. 1. Illustration of the synthesized pressure fields and the decoupled velocity estimation. On the left, the axial velocity component is estimated based on axial oscillations only. In the middle, the transverse velocity component is estimated based on two double-oscillation fields in the ZX plane. On the right, the double-oscillations occur in the ZY plane, from which the elevation velocity component is estimated. White areas indicate apodization values of 1 and black areas correspond to 0.

where the second is a spatially Hilbert transformed version of the first. Thereby, the lateral and elevation velocity components can be estimated based on spatial quadrature sampling.

The different apodizations needed to obtain the required fields can be applied in parallel, and hence, independently. Furthermore, it is assumed that the velocity estimation can be decoupled into estimating three independent velocity components: the axial, $v_{z'}$, transverse, $v_{x'}$, and elevation, $v_{y'}$, velocity components. The three estimated velocity components can be obtained, such that they are orthogonal in a primed coordinate system (x', y', z') which depends on the direction of the steered beam, as illustrated in Fig. 2.

B. Beamforming

The beamforming follows the steered beam approach described by the authors for a phased-array implementation [31]. The apodizations required to generate the double-oscillating fields are identical expect for a rotation of the receiving aperture of 90° in the transducer's XY plane. The beamforming approach is illustrated in Fig. 2. For each sample depth, five samples are beamformed: one along the center axis for conventional axial estimation, and two pairs of the left and right TO samples for spatial in-phase and quadrature (IQ) in both the transverse and elevation directions. All five samples are beamformed in parallel in receive, based on the same transmission. Therefore, the three velocity components are estimated simultaneously and from the same data set.

C. Velocity Estimation

Prior to the velocity estimation, matched filtration is used by convolving the simulated RF signals with the time-reversed emitted pulse. When clutter filtering (stationary echo cancelling) is applied, it is performed by subtracting the mean ensemble value.

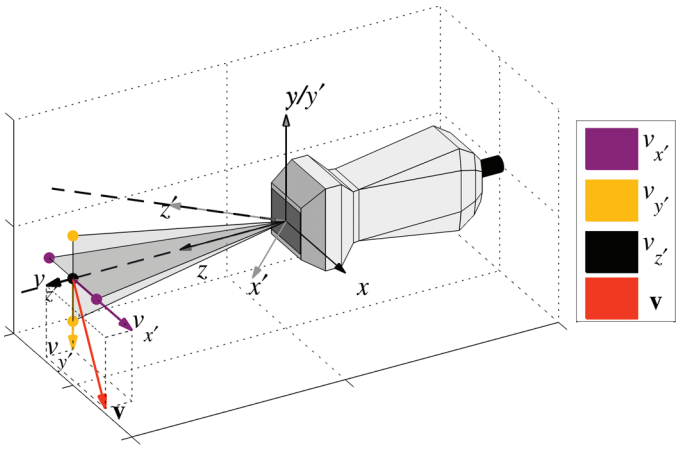

Fig. 2. Beamforming approach for 3-D velocity estimation using a 2-D matrix phased-array transducer. The coordinate system of the transducer is (x, y, z), and the sampling coordinate system along the direction of the steered beam is (x', y', z'). The dots indicate beamformed samples at a given depth: A center line is beamformed for conventional axial velocity $v_{z'}$ estimation, and two pairwise TO lines are beamformed for estimation of the transverse $v_{x'}$ velocity component and the elevation $v_{y'}$ velocity component.

The axial velocity component is calculated using an autocorrelation estimator [32] with RF averaging [33]. The estimation of the transverse and elevation velocity components, $v_{x'}$ and $v_{y'}$, follows the principle of the method by Jensen [34]. The velocity estimation is the same for $v_{x'}$ and $v_{y'}$, each based on one pair of the four TO lines. Based on the spatial quadrature and temporal quadrature in the ZX and ZY plane, $v_{x'}$ and $v_{y'}$ can be estimated.

RF averaging is performed by averaging the autocorrelation estimate over the length of the excitation pulse [33], [34]. The transverse λ_x and elevation λ_y wavelengths can be calculated theoretically [31]. Bias compensation may be performed by substituting λ_x and λ_y with, for instance, the mean lateral wavelengths, $\overline{\lambda}_x$ and $\overline{\lambda}_y$, which can be estimated based on simulations or measurements. Alternatively, the TO fields (i.e., the beamforming) can also be optimized, as described subsequently.

D. Optimizing the Method

The performance of the TO method can be optimized by ensuring a good agreement between the transverse wavelength, λ_x, used when beamforming the TO lines and the resulting $\overline{\lambda}_x$ in the combined TO field [31], [34]. Because the transverse wavelength is subsequently used in the velocity estimation, a mismatch between the expected wavelength and the actual wavelength in the field will lead to a biased estimate and a poorer standard deviation. The same holds for λ_y.

The theoretical description of the transverse wavelength is based on the theory of continuous wave fields, in which the emitting aperture function is related to the radial pressure field in the far-field region or the focal point by the Fourier transform [7]. Nonetheless, this serves as a good approximation of the actual mean frequency in the TO field. However, if a further optimization is desirable, simulations must be carried out to calculate the mean transverse frequency [34]. This is necessary because the complex relation between the beamforming, the transducer apodization, transmitted pulse, and the field cannot be described analytically.

To compensate for a potential bias of the velocity estimates when using the theoretical wavelength in the beamforming stage, the mean transverse wavelength $\overline{\lambda}_x$ should be used in the subsequent velocity estimation.

The best optimization with the lowest standard deviation, however, is obtained when 1) the TO field is optimized when beamforming and 2) the estimated mean wavelength is used in the velocity estimation. This approach was applied to obtain the presented results. In general, the optimization should be performed for each specific setup in question and (ideally) for each point in the image [35].

E. Number of Operations

The computational demands of the 3-D TO method are addressed in terms of the operations needed (both additions and multiplications) for performing the velocity estimation. For the numbers stated subsequently, it is assumed that the temporal quadrature data have already been obtained either by IQ sampling or by means of the Hilbert transform. For each set of four samples used for estimating $v_{x'}$ and $v_{y'}$, the following number of operations are required:

$$N_{\mathrm{c,TO}} = 52 + \frac{14}{N_i} < 53, \quad \text{if } N_i > 14,$$

where N_i is the ensemble length used in the velocity estimation. The required number of floating point operations per second (flops) can be calculated as

$$f_{\mathrm{flops}} = N_{\mathrm{c}} \cdot f_{\mathrm{s}} \cdot p_{\mathrm{v}},$$

where p_{v} is fraction of time used for velocity estimation.

Assuming N_i is 16, the sampling frequency is 15 MHz, and 80% of the time is used for flow acquisition, the required number of flops for estimating v_x and v_y is 0.64 Gflops. For comparison, the number of calculations needed by the conventional axial velocity estimator is 0.11 Gflops.

The number of calculations required for the two transverse velocities is approximately a factor of 6 larger than for the conventional estimator. For a realistic example, the combined flops required for estimating v_x, v_y, and v_z are 0.75 Gflops. This is well within the capabilities of standard CPUs today. Thus, a real-time implementation of the approach is feasible on a modern scanner.

F. Performance Metrics

The metrics employed for evaluating the performance of the method are described in the following. The metrics have previously been defined and described by Pihl *et al.* [31], and the reader is refereed to this reference for details.

The performance for the 3-D velocity vector estimation is determined by the precision and accuracy of the estimated velocity components. Therefore, the average of N_p velocity profiles is investigated. In the calculations of the relative mean standard deviations $\tilde{\sigma}$ and the relative mean biases $\tilde{B}$, it is assumed that the velocity estimates are independent. The normalization is obtained by dividing by the peak velocity magnitude ($v_0 = 1$ m/s).

For the most part, only the results for the transverse v_x and the elevation v_y velocity components are presented as the axial velocity component v_z is estimated using a well-established estimator as described previously.

III. Simulation Environment

The simulation studies performed to investigate the TO method for 3-D velocity vector estimation uses the ultrasound simulation program Field II [36], [37]. The simulation environment and the parameters are described in the following.

The simulation environment consists of several parameters. Some were kept constant and others were varied in a parameter study. The parameters are listed in the following with their default values, and the varied values are listed in Table I. The simulation study was performed with a sampling frequency, f_s, of 100 MHz, and a speed of sound, c, set to 1480 m/s to mimic the speed of sound in water.

A 2-D phased array transducer was emulated as a matrix array with a center frequency, f_0, of 3.5 MHz. The array had 32 × 32 elements with a pitch in both dimensions of 300 μm. The kerfs were set to $\lambda/100$, where λ is the wavelength of the ultrasound pulse in water. The one-way impulse response of the transducer was defined as a 2-cycle Hanning windowed pulse at the center frequency, yielding a 6-dB bandwidth of 96%.

The emitted pulse for the velocity vector estimation was an 8-cycle Hanning windowed sinusoid at the center frequency. The emitted ultrasound beam was a plane wave. As default, it was steered in the direction of the z-axis, but the steering angles, θ_{zx} and θ_{zy}, were varied in the parameter study. The default pulse repetition frequency, f_{prf}, was 1.5 kHz.

All 1024 channels were used for transmitting the pulse. The default was an apodization of 1 for all elements (rectangular). The receive aperture for the conventional axial velocity estimation was apodized with a circular symmetrical Hamming window. The receive apodization for both pairs of TO lines were two peaks with widths of w and spaced a given distance d apart. The apodization of the TO peaks was varied in both dimensions, i.e., in the direction with oscillations (osc.) and in the direction without oscillations (non-osc.). The difference between the pair of TO lines in the x-direction and the y-direction was merely a 90° rotation.

As default, an ensemble length of 32 emissions was used, and no noise was added to the simulated RF signals. When testing the effect of varying the SNR, zero-mean white Gaussian noise was added to the beamformed RF data before the match filtration. The amplitude of the noise was varied to obtain different SNR values. The matched filtration improved the SNR by 18 dB. The SNR values after the matched filtration are listed in Table I.

The flow phantom used for the simulations was defined as a 20 × 20 × 20 mm cube with a cylinder with a length l of 20 mm and a radius r of 6 mm centered inside the block. The scatterers inside the cylinder were moving with a circular symmetric parabolic velocity profile, and the scatterers outside the cylinder were stationary. The vessel boundary was not modeled. The ratio between the scattering amplitudes of the moving scatterers and the stationary scatterers was 1:100. The simulations were performed with a constant peak speed $|\vec{v}_0|$ of 1 m/s, while the direction of the flow $\vec{v}_0/|\vec{v}_0|$ was varied by rotating the block of scatterers. After the rotation, the block was translated to the desired depth. As default, the center of phantom was located at $(x, y, z) = (0, 0, 30)$ mm. The steering direction and the radial depth were varied. Depending on this, the block of scatterers were rotated and translated accordingly to obtain velocity vectors orthogonal to the ultrasound beam.

The direction of the flow was determined by two angles α and β as illustrated in Fig. 3. Both α and β were varied from 0° to 90° in steps of 15°. Thereby, 49 flow directions where simulated covering the positive octant of the unit sphere, which is representative for the whole unit sphere assuming the sign of the velocity components does not affect the velocity estimator. Note that only 43 of the directions are unique, because the direction for all seven values of α is the same when β is 90°.

For each parameter configuration, 3200 emissions with random scatterer initialization in terms of position and amplitude were simulated. This allowed the calculation of 100 independent profiles using an ensemble length of 32.

IV. Three-Dimensional Velocity Vector Profiles

This section presents the results of estimating three-dimensional velocities with various directionality in 3-D

TABLE I. Variables in Parameter Study.

Parameter	Values
Flow angle α [°]	**0**,15,...,90
Flow angle β [°]	**0**,15,...,90
Ensemble length	8,16,**32**,64
SNR [dB]	−6, −3,...12,∞
Steering angle θ_{zx} [°]	**0**,5,...,45
Steering angle θ_{zy} [°]	**0**,5,...,45
Transmit apodization (in 2-D)	Hanning, Tukey, **Rect**
TO peak apod. (osc. direction)	Hanning, Tukey, **Rect**
TO peak apod. (non-osc. direction)	Hanning, Tukey, **Rect**
No. of elements in TO peak spacing	8,12,16,20,**24**
No. of elements in TO peak width	2,4,**8**,12,16

Bold values correspond to the reference setup.

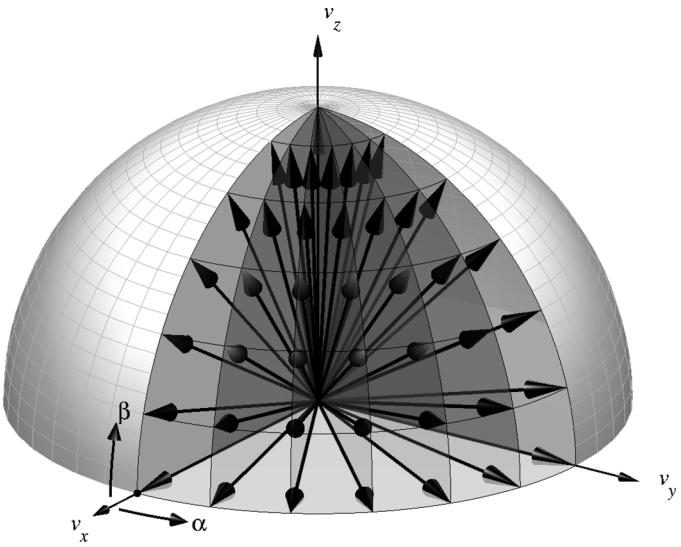

Fig. 3. The 49 (43 unique) simulated flow directions within the positive octant of the unit sphere. Note how the black arrows touch the intersections of the black lines.

space. The method estimates the velocities along an entire line (M-mode), thereby obtaining 3-D velocity profiles.

With the reference parameter values, the mean velocity profiles for four different flow directions are presented in Fig. 4. The figure shows that the estimated velocity profiles follow the true profiles, and that the standard deviations are higher for v_x and v_y compared with v_z. It can also be observed that the standard deviation for all three components gets larger as β is increased.

For a quantitative comparison, the performance metrics corresponding to the four flow directions are listed in Table II. The magnitude $\tilde{B}$ is 4% or smaller for all cases. It can also be observed that the standard deviations are higher for v_x and v_y compared with v_z. The increase in $\tilde{\sigma}$ with increasing β for all three velocity components, as observed in Fig. 4 and Table II, is addressed in the following. The f_{prf} was adjusted according to β to avoid aliasing of the axial velocity component. For an autocorrelation estimator, increasing the pulse repetition frequency or the magnitude of the velocity component yields a higher standard deviation [38]. Accordingly, the rise in $\tilde{\sigma}$ follows the increase in the pulse repetition frequency, because the normalization factor is kept constant.

Considering an autocorrelation velocity estimator and assuming a fixed relative velocity uncertainty $\Delta v/v_{\max}$ for a given setup, an increase in f_{prf}, and therefore $v_{\max}$, will not change the relative uncertainty. However, in absolute numbers, the uncertainty will increase, resulting in higher standard deviations if the normalization constant is not adjusted with the f_{prf}. This can be observed in the table, where $\tilde{\sigma}$ doubles when f_{prf} is doubled.

The preceding discussion demonstrates that to reduce the standard deviation of the velocity estimates, the pulse repetition frequency should be adjusted according to the individual velocity components.

V. Parameter Study

The previous section demonstrated the ability of the 3-D TO method to estimate 3-D velocity profiles. The following presents the results of varying the previously outlined parameters.

In the parameter study, the relative mean bias $\tilde{B}$ and relative mean standard deviations $\tilde{\sigma}$ are computed for each set of mean velocity profiles for the various parameter settings. This allows for a more straightforward comparison of the performance over the different parameters and their values. To reduce the effect of the vessel boundaries, the performance metrics are calculated over the entire vessel except for the outer most 1 mm at either end. The bias is mainly affected in the outermost region, because the velocity profile broadens in that area and extends into the stationary tissue. If these areas were still considered, a velocity profile that was accurate for the inner 90% would get a positive bias. That would give a wrong indication of the bias of the estimator. The broadening of the velocity estimates at the vessel boundaries in simulations arises from off-axis velocities when the vessel is rotated and clutter filtering is performed.

A. Flow Direction

The performance metrics presented in Fig. 5 are an extension of the results presented in the previous section. The relative mean bias and standard deviations are calculated with the normalization factor $v_0 = 1/\text{s}$. The figure reveals that the standard deviations increase as a function of β, because the increase in pulse repetition frequency is disregarded in the normalization. The range is 5% to 31% with a median of 18%. The shape of the individual curves is not affected by α. The relative mean bias ranges from -7% to 5%, with a median of -2% and is only slightly affected by β.

Additionally, the symmetry of the performance metrics for v_x and v_y can be appreciated. The performance for v_x at $\alpha = 0^\circ$ is similar to performance of v_y at $\alpha = 90^\circ$. This behavior is expected because the transducer is symmetric in the x- and y-dimensions.

B. Ensemble Length

The number of emissions per velocity estimate affects the performance. The results are shown in Fig. 6(a). As the number of emissions increases, the relative mean standard deviation decreases, e.g., when the ensemble length is increased from 16 to 64, $\tilde{\sigma}_{v_x}$ and $\tilde{\sigma}_{v_y}$ decrease from 7.4% and 13% to 4.5% and 6.2%, respectively. The decrease in standard deviation is expected because the standard deviation should decrease with a factor of $1/\sqrt{N_{\text{e}}}$, if the N_{e} signals are uncorrelated. The relative mean bias for v_x decreases from 10% to 1.5%, whereas the relative mean bias for v_y is unaffected.

TABLE II: PERFORMANCE METRICS FOR THE FOUR FLOW DIRECTIONS PRESENTED IN FIG. 4.

Metric	$[0,0]^\circ$	$[45,0]^\circ$	$[45,15]^\circ$	$[45,45]^\circ$	Unit
$\tilde{B}_{v_x}$	0.32	3.9	−2.8	−4.0	[%]
$\tilde{B}_{v_y}$	0.14	4.0	−2.5	−3.6	[%]
$\tilde{B}_{v_z}$	0.0003	0.020	−0.76	−2.2	[%]
$\tilde{\sigma}_{v_x}$	4.9	5.9	11	23	[%]
$\tilde{\sigma}_{v_y}$	8.1	6.3	11	25	[%]
$\tilde{\sigma}_{v_z}$	0.46	0.49	0.85	1.7	[%]
f_{prf}	1500	1500	3100	8400	[Hz]

C. SNR

The effect of varying the SNR is demonstrated in Fig. 6(b). Changing the SNR from ∞ to 0 dB increases the relative mean bias for v_x from 5% to 12% and for v_y from 8% to 14%. The TO approach breaks down for SNRs between −6 dB and −3 dB.

D. Steering Angles

Fig. 6(c) shows the result of changing the steering angle θ_{zx}. The results for θ_{zy} are similar and are therefore not shown. As the results indicate, the relative standard deviation is almost unaffected, with values between 5% and 7%. The relative mean biases vary from −2% to 2%. These

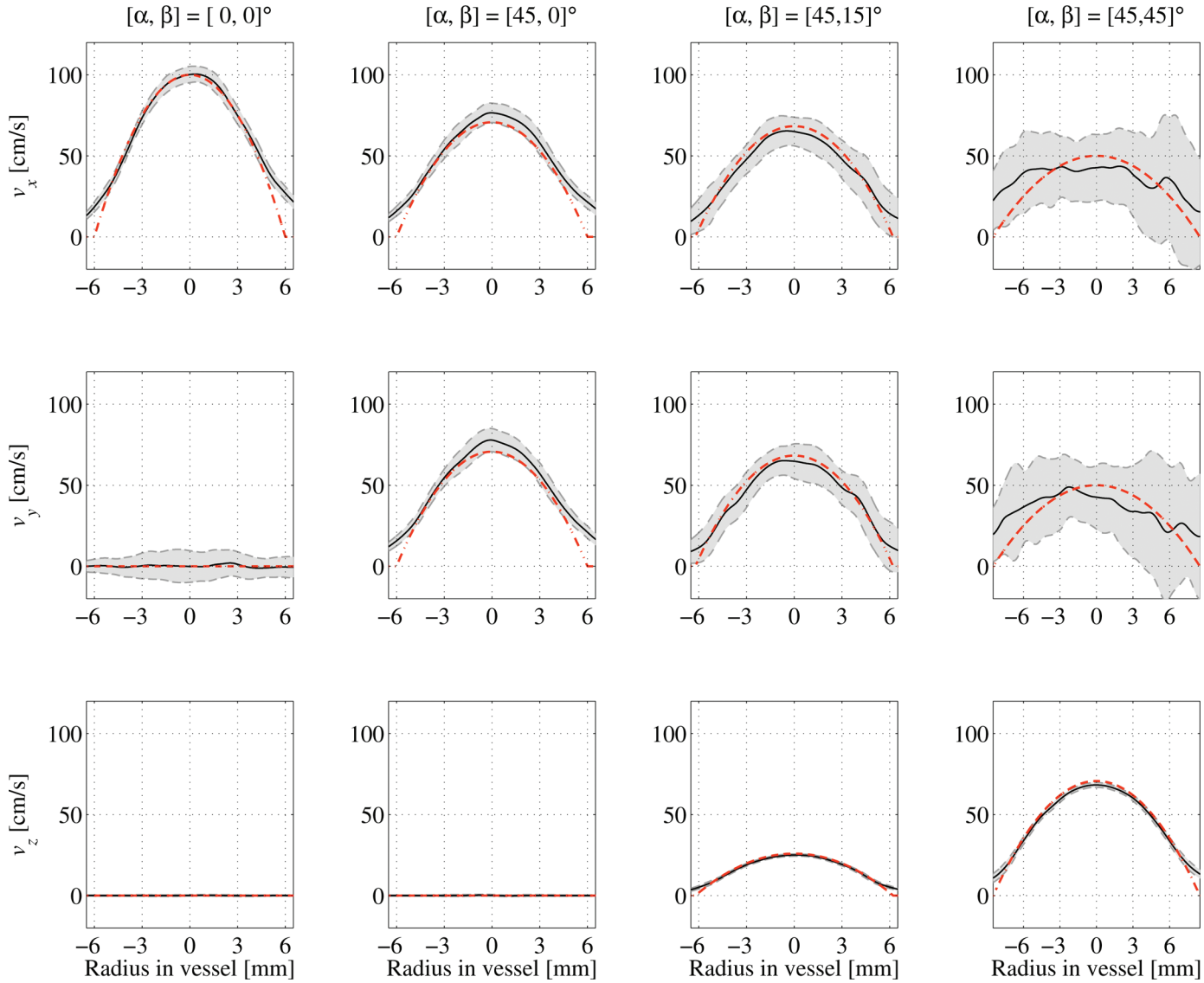

Fig. 4. Velocity estimates of v_x, v_y, and v_z at four different pairs of the flow angles $[\alpha, \beta]$. The dot-dashed lines indicate the true velocity, solid lines indicate the mean of 100 profiles, and the shaded area indicates the range of one standard deviation.

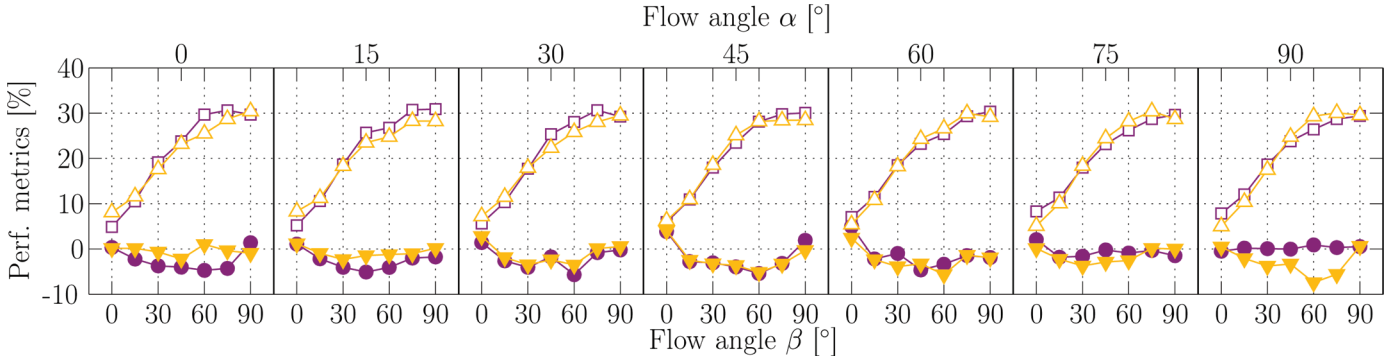

Fig. 5. Performance metrics as a function of the two flow angles α and β for the relative mean standard deviations $\tilde{\sigma}_{v_x}$ (open square) and $\tilde{\sigma}_{v_y}$ (open triangle), and the relative mean biases $\tilde{B}_{v_x}$ (filled circle) and $\tilde{B}_{v_y}$ (filled triangle).

values are obtained by using the theoretically calculated transverse and elevation wavelengths in the beamforming. The values for λ_x and λ_y increase as a function of steering angle because of the cosθ-term; however, the most accurate velocity estimates (with the smallest bias) were obtained using $\overline{\lambda}_x$ and $\overline{\lambda}_x$ calculated at steering angles of 0° in the velocity estimation. That observation and the low values for especially the relative mean standard deviations were surprising. It was expected that steering the beam would degrade the performance of the velocity estimator. An explanation may reside in the ideal conditions of the Field II simulation environment, and the fact that no noise is added. Hence, the drop in SNR caused by the angular sensitivity has not been captured. To test this hypothesis, the velocity estimation was repeated with white Gaussian noise added, so that the SNR was changed to 0 dB at a steering angle of 0°. The noise amplitude is kept constant for all steering angles. The result can be observed in Fig. 6(d). When the steering angle increases, the received energy is lower, and hence the SNR decreases if the noise is constant. The decrease in SNR degrades the performance and the relative mean standard deviations increases. The relative mean bias is only affected at large steering angles. The results thereby confirm the hypothesis that the drop in SNR degrades the performance when steering the beam.

E. Apodization

The result of changing the spacing of the TO peaks in the x-direction is illustrated in Fig. 6(e). As the spacing increases, the relative mean standard deviations decrease. The relative mean bias for v_y is 0% for almost all settings, but decreases for v_x. Fig. 6(f) shows the effect of changing the TO peak width in the x-direction. Increasing the TO peak width slightly increases the relative mean standard deviations. The relative mean bias for v_x has a flat parabolic shape. For v_y, the relative mean bias is unaffected. It should, however, be noted that this does not take the corresponding increase in SNR into consideration.

Fig. 6(g) presents the results of combining various apodization shapes. Three different apodization shapes are used: A Hanning window, a Tukey window with a ratio of taper of 0.5, and a rectangular window. These windows are applied to the transmitting aperture, the receive aperture with the TO peaks in the transverse oscillating direction, and with apodizations across the TO peaks in the non-oscillating direction. All 27 combinations are investigated. The first data point in Fig. 6(g) is denoted HHH. It is an abbreviation for applying Hanning, Hanning, and Hanning windowing in transmit, receive (oscillation direction), and receive (non-oscillation direction), respectively. The next point is HHT, denoting Hanning, Hanning, and Tukey, and the third data point is HHR, denoting Hanning, Hanning, and Rect. The fourth data point is HTH, and the pattern is repeated. The results indicate that the relative mean biases are practically unaffected, as well as the relative mean standard deviation for v_x. For v_y, however, the relative mean standard deviation has a serrated appearance. The relative standard deviation is around 7% when the apodization in the non-oscillating direction is a rectangular window, and it is about 5% when it is Hanning apodized.

When deciding on which apodization to use, it is important to remember that the SNR is proportional with the area under the apodization functions. The consideration of SNR and the area under the apodization functions is also important when considering the peak width. The results indicate that in a noisy environment, there will be a trade-off between the TO spacing, the TO peak width, and the apodization functions for which the SNR affects the optimal setting.

F. Summary

Overall, the parameter study demonstrates that the TO method is robust in terms of creating the TO fields and the appertaining transverse and elevation wavelengths in this setup. The theoretical values of the TO wavelengths can be used, but for bias optimization, the mean TO wavelengths based on the TO fields should be computed. Additionally, the TO fields themselves should be optimized to reduce the standard deviations of the velocity estimates. The optimization of the parameters should be done for each setup, and be dynamic based on depth and steering angles.

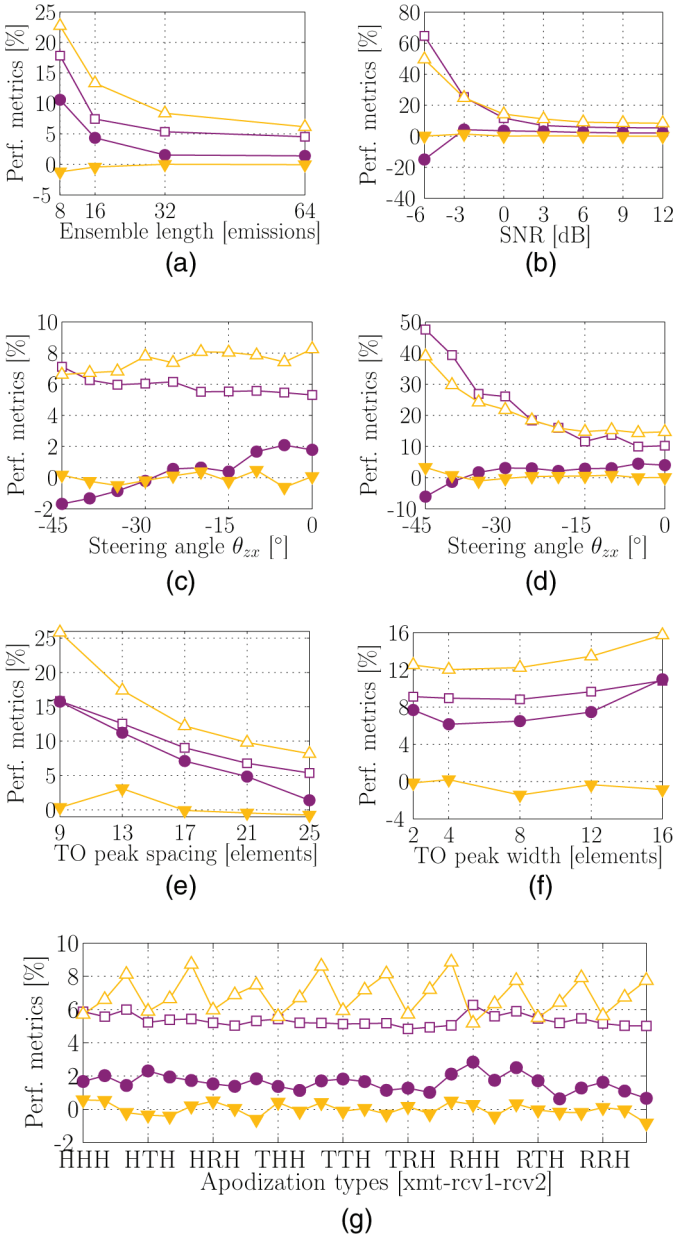

Fig. 6. Performance metrics as a function of various parameter settings and their values: The relative mean standard $\tilde{\sigma}_{v_x}$ (open square) and $\tilde{\sigma}_{v_y}$ (open triangle), and the relative mean biases $\tilde{B}_{v_x}$ (filled circle) and $\tilde{B}_{v_y}$ (filled triangle). The reader is referred to the text for further details.

VI. Conclusion

A method for estimating 3-D velocity vectors using a transverse oscillation approach has been presented. The method requires five beamformed IQ samples for a given ensemble length to estimate the three velocity components simultaneously and from the same data set. Because the velocity estimation only requires 0.75 Gflops, a real-time implementation on current commercial platforms is feasible.

The simulation study demonstrates that three-dimensional velocity profiles can be obtained regardless of the flow direction. In terms of accuracy, the magnitude of the relative mean bias for all 49 flow directions did not exceed 7% and was generally only a few percent. Neither α nor β influenced the bias substantially.

Regarding the precision, the standard deviations were unaffected by α, but rose as β increased. Normalizing with a fixed velocity, the increase was reflected in the relative mean standard deviations, which ranged from 5% to 31%. For comparison, the range was 2% to 3% for v_z.

The simulation study revealed the effect of several parameters, including the SNR, steering angle, and apodization types. In terms of noise, the velocity estimation broke down for SNRs between −6 and −3 dB. Overall, the results demonstrate that 3-D TO method is able to estimate the three velocity components under various parameter settings. However, the parameters should be optimized for each specific setup and as a function of steering angle and depth to reduce the bias and standard deviation of the velocity estimates.

Besides requiring a 2-D phased-array matrix transducer, the complexity of the 3-D TO method is within the capabilities of modern scanners. The simulation results presented are promising, and they warrant further investigation and experimental verification. That is the topic of the accompanying paper on measured 3-D vector velocity profiles [29].

References

[1] D. H. Evans, J. A. Jensen, and M. B. Nielsen, "Ultrasonic colour Doppler imaging," *Interface Focus*, vol. 1, no. 4, pp. 490–502, 2011.

[2] E. G. Grant, C. B. Benson, G. L. Moneta, A. V. Alexandrov, J. D. Baker, E. I. Bluth, B. A. Carroll, M. Eliasziw, J. Gocke, B. S. Hertzberg, S. Katanick, L. Needleman, J. Pellerito, J. F. Polak, K. S. Rholl, D. L. Wooster, and R. E. Zierler, "Carotid artery stenosis: Gray-scale and Doppler US diagnosis—Society of Radiologists in Ultrasound consensus conference," *Radiology*, vol. 229, no. 2, pp. 340–346, 2003.

[3] C. Arning, B. Widder, G. M. von Reutern, H. Stiegler, and M. Görtler, "Revision of DEGUM ultrasound criteria for grading internal carotid artery stenoses and transfer to NASCET measurement," *Ultraschall Med.*, vol. 31, no. 3, pp. 251–257, 2010.

[4] B. Dunmire, K. W. Beach, K.-H. Labs, M. Plett, and D. E. Strandness, "Cross-beam vector Doppler ultrasound for angle independent velocity measurements," *Ultrasound Med. Biol.*, vol. 26, no. 8, pp. 1213–1235, 2000.

[5] R. Steel, K. V. Ramnarine, F. Davidson, P. J. Fish, and P. R. Hoskins, "Angle-independent estimation of maximum velocity through stenoses using vector Doppler ultrasound," *Ultrasound Med. Biol.*, vol. 29, no. 4, pp. 575–584, 2003.

[6] P. Tortoli, A. Dallai, E. Boni, L. Francalanci, and S. Ricci, "An automatic angle tracking procedure for feasible vector Doppler blood velocity measurements," *Ultrasound Med. Biol.*, vol. 36, no. 3, pp. 488–496, 2010.

[7] J. A. Jensen and P. Munk, "A new method for estimation of velocity vectors," *IEEE Trans. Ultrason. Ferroelectr. Freq. Control*, vol. 45, no. 3, pp. 837–851, 1998.

[8] J. A. Jensen, M. J. Pihl, J. B. Olesen, P. M. Hansen, K. L. Hansen, and M. B. Nielsen, "New developments in vector velocity imaging using the transverse oscillation approach," in *Proc. SPIE Med. Imag.*, vol. 8675, art. no. 86750F, 2013.

[9] L. J. Frazin, G. Lanza, M. Vonesh, F. Khasho, C. Spitzzeri, S. McGee, D. Mehlman, K. B. Chandran, J. Talano, and D. McPherson, "Functional chiral asymmetry in descending thoracic aorta," *Circulation*, vol. 82, no. 6, pp. 1985–1994, 1990.

[10] P. Tortoli, V. Michelassi, G. Bambi, F. Guidi, and D. Righi, "Interaction between secondary velocities, flow pulsation and vessel

morphology in the common carotid artery," *Ultrasound Med. Biol.*, vol. 29, no. 3, pp. 407–415, 2003.
[11] K. L. Hansen, J. Udesen, F. Gran, J. A. Jensen, and M. B. Nielsen, "In-vivo examples of complex flow patterns with a fast vector velocity method," *Ultraschall Med.*, vol. 30, no. 5, pp. 471–477, 2009.
[12] P. J. Kilner, G. Z. Yang, R. H. Mohiaddin, D. N. Firmin, and D. B. Longmore, "Helical and retrograde secondary flow patterns in the aortic arch studied by three-directional magnetic resonance velocity mapping," *Circulation*, vol. 88, no. 5, pp. 2235–2247, 1993.
[13] A. Harloff, F. Albrecht, J. Spreer, A. F. Stalder, J. Bock, A. Frydrychowicz, J. Schollhorn, A. Hetzel, M. Schumacher, J. Hennig, and M. Markl, "3D blood flow characteristics in the carotid artery bifurcation assessed by flow-sensitive 4D MRI at 3T," *Magn. Reson. Med.*, vol. 61, no. 1, pp. 65–74, 2009.
[14] C. Taylor, T. Hughes, and C. Zarins, "Finite element modeling of blood flow in arteries," *Comput. Methods Appl. Mech. Eng.*, vol. 158, no. 1, pp. 155–196, 1998.
[15] D. A. Steinman, J. B. Thomas, H. M. Ladak, J. S. Milner, B. K. Rutt, and J. D. Spence, "Reconstruction of carotid bifurcation hemodynamics and wall thickness using computational fluid dynamics and MRI," *Magn. Reson. Med.*, vol. 47, no. 1, pp. 149–159, 2002.
[16] R. E. Daigle, C. W. Miller, M. B. Histand, F. D. McLeod, and D. E. Hokanson, "Nontraumatic aortic blood flow sensing by use of an ultrasonic esophageal probe," *J. Appl. Phys.*, vol. 38, no. 6, pp. 1153–1160, 1975.
[17] M. D. Fox, "Multiple crossed-beam ultrasound Doppler velocimetry," *IEEE Trans. Sonics Ultrason.*, vol. SU-25, no. 5, pp. 281–286, 1978.
[18] V. L. Newhouse, K. S. Dickerson, D. Cathignol, and J.-Y. Chapelon, "Three-dimensional vector flow estimation using two transducers and spectral width," *IEEE Trans. Ultrason. Ferroelectr. Freq. Control*, vol. 41, no. 1, pp. 90–95, 1994.
[19] O. Bonnefous, "Measurement of the complete (3D) velocity vector of blood flows," in *Proc. IEEE Ultrason. Symp.*, 1988, pp. 795–799.
[20] I. A. Hein, "Triple-beam lens transducers for three-dimensional ultrasonic fluid flow estimation," *IEEE Trans. Ultrason. Ferroelectr. Freq. Control*, vol. 42, no. 5, pp. 854–869, 1995.
[21] J. A. Jensen, "Directional velocity estimation using focusing along the flow direction: I: Theory and simulation," *IEEE Trans. Ultrason. Ferroelectr. Freq. Control*, vol. 50, no. 7, pp. 857–872, 2003.
[22] G. E. Trahey, J. W. Allison, and O. T. von Ramm, "Angle independent ultrasonic detection of blood flow," *IEEE Trans. Biomed. Eng.*, vol. BME-34, no. 12, pp. 965–967, 1987.
[23] J. Meunier, "Tissue motion assessment from 3D echographic speckle tracking," *Phys. Med. Biol.*, vol. 43, no. 5, pp. 1241–1254, 1998.
[24] M. Crapper, T. Bruce, and C. Gouble, "Flow field visualization of sediment-laden flow using ultrasonic imaging," *Dyn. Atmos. Oceans*, vol. 31, no. 1–4, pp. 233–245, 2000.
[25] H. B. Kim, J. R. Hertzberg, and R. Shandas, "Development and validation of echo PIV," *Exp. Fluids*, vol. 36, no. 3, pp. 455–462, 2004.
[26] L. Liu, H. Zheng, L. Williams, F. Zhang, R. Wang, J. Hertzberg, and R. Shandas, "Development of a custom-designed echo particle image velocimetry system for multi-component hemodynamic measurements: System characterization and initial experimental results," *Phys. Med. Biol.*, vol. 53, no. 5, pp. 1397–1412, 2008.
[27] C. Poelma, J. M. Mari, N. Foin, M. Tang, R. Krams, C. G. Caro, P. D. Weinberg, and J. Westerweel, "3D flow reconstruction using ultrasound PIV," *Exp. Fluids*, vol. 50, no. 4, pp. 777–785, 2011.
[28] G. R. Bashford and O. T. von Ramm, "Ultrasound three-dimensional velocity measurements by feature tracking," *IEEE Trans. Ultrason. Ferroelectr. Freq. Control*, vol. 43, no. 3, pp. 376–384, 1996.
[29] M. J. Pihl, M. B. Stuart, B. G. Tomov, M. F. Rasmussen, and J. A. Jensen, "A transverse oscillation approach for estimation of three-dimensional velocity vectors. Part II: Experimental validation," *IEEE Trans. Ultrason. Ferroelectr. Freq. Control*, vol. 61, no. 10, pp. 1608–1618, 2014.
[30] M. E. Anderson, "Multi-dimensional velocity estimation with ultrasound using spatial quadrature," *IEEE Trans. Ultrason. Ferroelectr. Freq. Control*, vol. 45, no. 3, pp. 852–861, 1998.
[31] M. J. Pihl, J. Marcher, and J. A. Jensen, "Phased-array vector velocity estimation using transverse oscillations," *IEEE Trans. Ultrason. Ferroelectr. Freq. Control*, vol. 59, no. 12, pp. 2662–2675, 2012.
[32] C. Kasai, K. Namekawa, A. Koyano, and R. Omoto, "Real-time two-dimensional blood flow imaging using an autocorrelation technique," *IEEE Trans. Sonics Ultrason.*, vol. 32, no. 3, pp. 458–463, 1985.
[33] T. Loupas, J. T. Powers, and R. W. Gill, "An axial velocity estimator for ultrasound blood flow imaging, based on a full evaluation of the Doppler equation by means of a two-dimensional autocorrelation approach," *IEEE Trans. Ultrason. Ferroelectr. Freq. Control*, vol. 42, no. 4, pp. 672–688, 1995.
[34] J. A. Jensen, "A New Estimator for Vector Velocity Estimation," *IEEE Trans. Ultrason. Ferroelectr. Freq. Control*, vol. 48, no. 4, pp. 886–894, 2001.
[35] J. A. Jensen, "Optimization of transverse oscillating fields for vector velocity estimation with convex arrays," in *Proc. IEEE Ultrason. Symp.*, July 2013, pp. 1753–1756.
[36] J. A. Jensen, "Field: A program for simulating ultrasound systems," *Med. Biol. Eng. Comput.*, vol. 34, suppl. 1, pt. 1, pp. 351–353, 1996.
[37] J. A. Jensen and N. B. Svendsen, "Calculation of pressure fields from arbitrarily shaped, apodized, and excited ultrasound transducers," *IEEE Trans. Ultrason. Ferroelectr. Freq. Control*, vol. 39, no. 2, pp. 262–267, 1992.
[38] J. A. Jensen, *Estimation of Blood Velocities Using Ultrasound: A Signal Processing Approach*. New York, NY: Cambridge University Press, 1996.

Michael J. Pihl was born in 1983. He received his M.Sc. degree in biomedical engineering in 2009 from the Technical University of Denmark (DTU) and the University of Copenhagen, Denmark. In 2007, he spent seven months at the Biomedical Engineering Department at Duke University, Durham, NC, researching ultrasonic clutter. In 2012, he earned his Ph.D. degree in biomedical engineering at the Center for Fast Ultrasound Imaging at DTU, where he is currently a postdoctoral associate. His main research area is ultrasonic velocity estimation—in particular the estimation of all three spatial velocity components. His other interests include medical imaging and digital signal processing.

Jørgen Arendt Jensen earned his Master of Science degree in electrical engineering in 1985 and the Ph.D. degree in 1989, both from the Technical University of Denmark. He received the Dr.Techn. degree from the university in 1996. He has published more than 250 journal and conference papers on signal processing and medical ultrasound and the book *Estimation of Blood Velocities Using Ultrasound*, published by Cambridge University Press in 1996. He is also developer of the Field II simulation program. He has been a visiting scientist at Duke University, Stanford University, and the University of Illinois at Urbana-Champaign. He is currently full professor of Biomedical Signal Processing at the Technical University of Denmark at the Department of Electrical Engineering and head of Center for Fast Ultrasound Imaging. He has given courses on blood velocity estimation at both Duke University and the University of Illinois and teaches biomedical signal processing and medical imaging at the Technical University of Denmark. He has given several short courses on simulation, synthetic aperture imaging, and flow estimation at international scientific conferences. He has received several awards for his research and is an IEEE Fellow. His research is centered on simulation of ultrasound imaging, synthetic aperture imaging, vector blood flow estimation, and construction of ultrasound research systems.